Available online at www.sciencedirect.com
ScienceDirect
Journal of Hydrodynamics
2010,22(6):838-846
DOI: 10.1016/S1001-6058(09)60124-4
www.sciencedirect.com/science/journal/10016058

A MULTIGRID-ACCELERATED THREE-DIMENSIONAL TRANSIENT-FLOW CODE AND ITS APPLICATION TO A NEW TEST PROBLEM*

KUMAR D. Santhosh
School of Mechanical and Building Science, Vellore Institute of Technology, Vellore-632014, India
DASS Anoop K.
Department of Mechanical Engineering, Indian Institute of Technology Guwahati, Guwahati-781039, India
DEWAN Anupam
Department of Applied Mechanics, Indian Institute of Technology Delhi Hauz Khas, New Delhi-110016, India,
E-mail: adewan@am.iitd.ac.in

(Received August 26, 2009, Revised August 10, 2010)

Abstract: A multigrid-assisted solver for the three-dimensional time-dependent incompressible Navier-Stokes equations on graded Cartesian meshes is developed. The spatial accuracy is third-order for the convective terms and fourth-order for the viscous terms, and a fractional-step strategy ensures second-order time accuracy. To achieve good time-wise efficiency a multigrid technique is used to solve the highly time-consuming pressure-Poisson equation that requires to be solved at every time step. The speed-up achieved by multigrid is shown in tabular form. The performance and accuracy of the code are first ascertained by computing the flow in a single-sided lid-driven cubic cavity with good grid-economy and comparing the results available in the literature. The code, thus validated, is then applied to a new test problem we propose and various transient and asymptotically obtained steady-state results are presented. Given the care taken to establish the credibility of the code and the good spatio-temporal accuracy of the discretization, these results are accurate and may be used for ascertaining the performance of any computational algorithm applied to this test problem.

Key words: incompressible flows, three-dimensional cavity flow, fractional-step method, multigrid method, Taylor-Gotler-Like (TGL) vortices, grid transformation

1. Introduction

The flow of an incompressible fluid in a lid-driven cubic cavity has been used extensively by numerical modelers as a test case for newly developed computational schemes. Its simple geometry and easily posed boundary conditions have made this flow a popular test case for computational schemes, giving rise to a need for an accurate database against which such schemes may be validated.

Three-dimensional cavity flows, which are more complex, realistic and general, have been an interesting research topic during the last three decades. Most earlier 3D simulations[1-5] in a cubic cavity emphasized on steady results. There are only a few works that dealt with transient solutions of the 3-D lid-driven cavity flows. Tang et al.[6] and Guermond et al.[7] produced transient results for the cubic lid-driven cavity at various Reynolds numbers. A discussion on the formation of a pair of Taylor-Gotler-Like (TGL) vortices at $Re = 1000$ may be found in these works. Recently, Beya and Lili[8] numerically solved the three-dimensional two-sided non-facing lid-driven cavity flows for various Reynolds numbers using the projection method. They employed full multigrid method for solving the Poisson equation on a staggered grid system using the finite volume method.

The unsteady incompressible flows occur frequently in problems of academic interest and engineering applications and one approach adopted for the solution of the unsteady, incompressible Navier-Stokes equations is the fractional-step method[9-12]. The finite difference method is frequently used in computational fluid dynamics. The method

* **Biography:** KUMAR D. Santhosh (1979-), Male, Ph. D., Associate Professor

essentially involves setting up a suitable grid in the problem domain, discretizing the governing equations with respect to the grid and solving them numerically. The common practice is to use a uniform grid, though it may not be the most appropriate one for an efficient computation. An accurate spatial resolution of the solution requires that grid points are clustered in the regions of large gradients. Hence nonuniform grids are used for many flow configurations. Finite difference formulations generally cannot be directly applied to nonuniform grids. The usual approach adopted is to map the physical space with a nonuniform grid on to a computational space with a uniform grid where a transformed set of equations is first solved before mapping this solution back onto the physical space for interpretation. By the use of nonuniform grids it is possible to cluster the grid lines in the regions of sharp gradients like shear-layers and use a relatively coarser grid in the regions involving small gradients, thus obtaining a good spatial scale resolution with a small overall grid size. This is the reason why graded Cartesian meshes are used in the present work to obtain good resolution of the wall-bounded and free-shear layers.

The transformed governing equations contain a larger number of terms than the original equations, which may result in some increase in the computational cost. Particularly, in the computation of transient flows, the pressure-Poisson equation that requires very accurate solution at every time step and consumes more than eighty percent of the total computational time needs special attention and an efficient algorithm for its numerical solution is highly desirable. The multigrid method which is arguably the best general convergence acceleration technique[13] is used in the present article to solve the pressure-Poisson equation numerically. Here the performance of multigrid method in the numerical solution of the pressure-Poisson equation on graded Cartesian meshes is examined in some details. Expectedly multigrid accelerates the convergence of the Gauss-Seidel iterations significantly, which in turn brings about a substantial reduction in the computational cost in the overall transient flow computation.

Thus it can be summarized that the main purpose of the present article is to develop a useful and efficient numerical tool for computing incompressible transient-viscous flows using multigrid method on graded Cartesian meshes and also to record our experiences on the application of multigrid to nonuniform meshes through the two problems studied, including the one-sided and two-sided 3-D lid-driven cavity problems. Other aims of this work are to carry out a comparison of the transient and steady-state results between 2-D and 3-D geometries and apply the present code to produce accurate transient and steady results for a new test case in the shape of the two-sided 3-D lid-driven cavity problem.

The article is organized in seven sections. Section 2 describes the governing equations in the physical plane (x, y, z) and computational plane (ξ, η, ζ). Section 3 gives a brief description of the fractional-step method employed and Section 4 provides some basics of the multigrid algorithm. Section 5 deals with the numerical method and Section 6 with the new test problem. Finally in Section 7 we list our observations and conclusions.

2. Governing equations

The 3-D unsteady, incompressible N-S equations in the primitive variable formulation and non-dimensional form can be written as

$$\frac{\partial u}{\partial x}+\frac{\partial v}{\partial y}+\frac{\partial w}{\partial z}=0 \tag{1}$$

$$\frac{\partial u}{\partial t}+\frac{\partial \left(u^2\right)}{\partial x}+\frac{\partial \left(uv\right)}{\partial y}+\frac{\partial \left(uw\right)}{\partial z}=-\frac{\partial p}{\partial x}+\frac{1}{Re}\left(\frac{\partial^2 u}{\partial x^2}+\frac{\partial^2 u}{\partial y^2}+\frac{\partial^2 u}{\partial z^2}\right) \tag{2}$$

$$\frac{\partial v}{\partial t}+\frac{\partial \left(uv\right)}{\partial x}+\frac{\partial \left(v^2\right)}{\partial y}+\frac{\partial \left(vw\right)}{\partial z}=-\frac{\partial p}{\partial y}+\frac{1}{Re}\left(\frac{\partial^2 v}{\partial x^2}+\frac{\partial^2 v}{\partial y^2}+\frac{\partial^2 v}{\partial z^2}\right) \tag{3}$$

$$\frac{\partial w}{\partial t}+\frac{\partial \left(uw\right)}{\partial x}+\frac{\partial \left(vw\right)}{\partial y}+\frac{\partial \left(w^2\right)}{\partial z}=-\frac{\partial p}{\partial z}+\frac{1}{Re}\left(\frac{\partial^2 w}{\partial x^2}+\frac{\partial^2 w}{\partial y^2}+\frac{\partial^2 w}{\partial z^2}\right) \tag{4}$$

Here u, v and w denote the velocities along the x, y and z directions respectively, t the time and p the pressure. The solution of governing Eqs.(1) - (4) on the graded Cartesian meshes using the finite difference method makes it necessary to transform the equations from the physical to the computational planes. The details of the transformation are presented in the next subsection.

2.1 *Transformation of governing equations*

It may be noted that when the governing Eqs.(1)

- (4) are transformed from the physical plane to a computational plane in which the mesh is uniform, the mathematical characteristics of the equations do not change. The transformed version of the governing equations is then solved in the computational plane by a higher order approximation and mapping of the results back to the physical plane is done. The transformation from the physical (x, y, z) plane to the computational (ξ, η, ζ) plane is of the form

$$\xi = \xi(x,y,z),\ \ \eta = \eta(x,y,z),\ \ \zeta = \zeta(x,y,z) \tag{5}$$

Using the transformations the governing equations in the computational plane can now be written as

$$\xi_x \frac{\partial u}{\partial \xi} + \eta_y \frac{\partial v}{\partial \eta} + \zeta_z \frac{\partial w}{\partial \zeta} = 0 \tag{6}$$

$$\frac{\partial u}{\partial t} + (u\xi_x)\frac{\partial u}{\partial \xi} + (v\eta_y)\frac{\partial u}{\partial \eta} + (w\zeta_z)\frac{\partial u}{\partial \zeta} =$$

$$-\xi_x \frac{\partial p}{\partial \xi} + \frac{1}{Re}\left(\xi_{xx}\frac{\partial u}{\partial \xi} + \xi_x^2 \frac{\partial^2 u}{\partial \xi^2}\right) +$$

$$\frac{1}{Re}\left(\eta_{yy}\frac{\partial u}{\partial \eta} + \eta_y^2 \frac{\partial^2 u}{\partial \eta^2}\right) +$$

$$\frac{1}{Re}\left(\zeta_{zz}\frac{\partial u}{\partial \zeta} + \zeta_y^2 \frac{\partial^2 u}{\partial \zeta^2}\right) \tag{7}$$

$$\frac{\partial v}{\partial t} + (u\xi_x)\frac{\partial v}{\partial \xi} + (v\eta_y)\frac{\partial v}{\partial \eta} + (w\zeta_z)\frac{\partial v}{\partial \zeta} =$$

$$-\eta_y \frac{\partial p}{\partial \eta} + \frac{1}{Re}\left(\xi_{xx}\frac{\partial v}{\partial \xi} + \xi_x^2 \frac{\partial^2 v}{\partial \xi^2}\right) +$$

$$\frac{1}{Re}\left(\eta_{yy}\frac{\partial v}{\partial \eta} + \eta_y^2 \frac{\partial^2 v}{\partial \eta^2}\right) +$$

$$\frac{1}{Re}\left(\zeta_{zz}\frac{\partial v}{\partial \zeta} + \zeta_z^2 \frac{\partial^2 v}{\partial \zeta^2}\right) \tag{8}$$

$$\frac{\partial w}{\partial t} + (u\xi_x)\frac{\partial w}{\partial \xi} + (v\eta_y)\frac{\partial w}{\partial \eta} + (w\zeta_z)\frac{\partial w}{\partial \zeta} =$$

$$-\zeta_z \frac{\partial p}{\partial \zeta} + \frac{1}{Re}\left(\xi_{xx}\frac{\partial w}{\partial \xi} + \xi_x^2 \frac{\partial^2 w}{\partial \xi^2}\right) +$$

$$\frac{1}{Re}\left(\eta_{yy}\frac{\partial w}{\partial \eta} + \eta_y^2 \frac{\partial^2 w}{\partial \eta^2}\right) +$$

$$\frac{1}{Re}\left(\zeta_{zz}\frac{\partial w}{\partial \zeta} + \zeta_z^2 \frac{\partial^2 w}{\partial \zeta^2}\right) \tag{9}$$

3. Fractional-step procedure

The four-step fractional-step method[10] employed in the present article is now described in some detail. In the first step the momentum Eq.(10) is solved for an auxiliary velocity field u_i using the pressure from the previous time step, the convective terms and viscous terms are solved explicitly using the second-order Adams-Bashforth method.

$$\frac{\hat{u}_i - u_i^n}{\Delta t} = -\frac{\partial p^n}{\partial x_i} + \frac{1}{2}\left[3H(u_i^n) - H(u_i^{n-1})\right] \tag{10}$$

where H is an operator representing the discretized convective and diffusive terms. In the second step Eq.(11) is solved to advance the auxillary velocity field $\hat{u}_i$ to u_i^* which is, of course, not divergence-free.

$$\frac{u_i^* - \hat{u}_i}{\Delta t} = \frac{\partial p^n}{\partial x_i} \tag{11}$$

In the third step, the incompressibility condition is enforced by solving the pressure Poisson Eq.(12), which is obtained by taking the divergence of Eq.(13) satisfying continuity equation for the next time step.

$$\frac{\partial}{\partial x_i}\frac{\partial p^{n+1}}{\partial x_i} = \frac{1}{\Delta t}\frac{\partial u_i^*}{\partial x_i} \tag{12}$$

Finally in the fourth step the velocity which satisfies the incompressibility condition is obtained by using the following correction step:

$$\frac{(u_i^{n+1} - u_i^*)}{\Delta t} = -\frac{\partial p^{n+1}}{\partial x_i} \tag{13}$$

The Poisson equation in the physical plane is given by Eq.(12) in the tensor form. This equation in the

transformed plane, solved using the multigrid method at each time step to satisfy the divergence-free condition, may be written in the expanded form as

$$\xi_x^2 \frac{\partial^2 p}{\partial \xi^2} + \eta_{yy} \frac{\partial p}{\partial \eta} + \eta_y^2 \frac{\partial^2 p}{\partial \eta^2} + \zeta_{xx} \frac{\partial p}{\partial \zeta} + \zeta_x^2 \frac{\partial^2 p}{\partial \zeta^2} = \sigma \quad (14)$$

where σ denotes the source term with the form

$$\frac{1}{\Delta t}\left(\xi_x \frac{\partial u^*}{\partial \xi} + \eta_y \frac{\partial v^*}{\partial \eta} + \zeta_z \frac{\partial w^*}{\partial \zeta} \right)$$

The pressure Poisson equation (Eq.(12)) is derived by taking the divergence of the intermediate velocity field Eq.(13) denoted by " * " subjected to the continuity constraint for the next time step. For computing the transient flow accurately the pressure Poisson equation has to be solved accurately at every time step. As is opposed to the solution of the transient momentum Eqs.(7) - (9), which is a relatively simple matter with an explicit technique, the solution of the pressure Poisson Eq.(14) is a nontrivial task that consumes almost 90% of the total CPU time required to update the primitive variables over one time step. For an efficient computation of transient flow using the pressure-velocity formulation it is therefore imperative that this equation is solved with an algorithm involving low computational cost. Here we use a four-level V-cycle multigrid method to solve the pressure Poisson equation.

4. Description of multigrid algorithm

The multigrid method has been chosen to accelerate the convergence rate, as it is highly suitable for elliptic equations such as the Poisson equation. There are two broad categories of multigrid methods: (1) Correction Schemes (CS) and (2) Full Approximation Schemes (FAS). The correction scheme is applicable to linear systems only. It involves corrections to the solution on coarse grids, which are eventually added to the fine-grid solution. As the Poisson equation is a linear equation, the correction scheme is used in the present work.

4.1 *Linear two-grid algorithm*

A two-grid algorithm for linear problems consists of smoothing on the fine grid, approximation of the required correction on the coarse grid, prolongation of the coarse grid correction to the fine grid and again smoothing on the fine grid. Let the equation to be solved is $\Delta^2 p = S$ where S denotes the source term. This equation after discretization by the finite difference method can be written as $L(p)_{i,j} = S_{i,j}$, where L denotes the Laplacian operator. A two-grid correction scheme is described below:

(1) Perform n iterations on a fine grid, $L(p)_{i,j} = S_{i,j}$.

(2) Compute the residual $R^f_{i,j} = L(p)_{i,j} - S_{i,j}$ and store at each point. This residual is restricted to the next coarser grid so that their lower frequency error components can be smoothened and the restricted residual is denoted by $I^c_f R^f_{i,j}$.

(3) The correction equation, given by

$$L(\Delta p)^c_{i,j} = -I^c_f R^f_{i,j} \quad (15)$$

is iterated few times on the coarser grid using zero as the initial guess while keeping the residual fixed at each grid point. The solution $\Delta p_{i,j}$ represents the correction to the fine-grid solution.

(4) The corrections obtained on the coarsest grid are prolongated on to the next finer grid and denoted by $I^f_c (\Delta p)^c_{i,j}$

(5) Correct the fine grid approximations using $p^{\text{new}}_{i,j} = p^{\text{old}}_{i,j} + I^f_c (\Delta p)^c_{i,j}$. It is necessary to repeat the above two-level cycle until desired convergence is achieved.

5. Numerical method

The governing equations are discretized in space, using a finite difference formulation on a staggered, Cartesian grid, where velocities and pressure are calculated at different locations. The main advantage of the staggered grid arrangement is the strong coupling between the pressure and velocities without requiring special interpolation techniques. This helps avoid convergence problems and oscillations in pressure fields. Another advantage of using the staggered grid for incompressible flows is that the pressure boundary conditions are not required when the momentum equations are evaluated. For the pressure Poisson equation, the pressure gradient normal to the walls is assumed zero, i.e.,

$$\frac{\partial p}{\partial x_i} = 0 \quad (16)$$

The convective terms of the momentum equations are approximated with Kuwahara's third-order upwind scheme[14] (Eq.(17)) and viscous terms are discretized with a fourth-order central-difference scheme (Eq.(18))

as given below:

$$\left(u\frac{\partial u}{\partial \xi}\right)_{i,j}=\frac{u_{i,j}\left(u_{i-2,j}-8u_{i-1},j+8u_{i+1,j}-u_{i+2,j}\right)}{12\Delta\xi}+$$

$$\frac{\left|u_{i,j}\right|\left(u_{i-2,j}-4u_{i-1,j}+6u_{i,j}-4u_{i+1,j}+u_{i+2,j}\right)}{4\Delta\xi} \tag{17}$$

$$\left(\frac{\partial^2 u}{\partial \xi^2}\right)_{i,j}=$$

$$\frac{-u_{i-2,j}+16u_{i-1,j}-30u_{i,j}+16u_{i+1,j}-u_{i+2,j}}{12\left(\Delta\xi\right)^2} \tag{18}$$

6. Computations, results and discussions

The code is based on the fractional-step method for the time integration of 3-D N-S equations. The performance of the code is already evaluated by the same authors in regard to time-wise efficiency and accuracy[15]. The results show that the 2-D code is capable of capturing transient results accurately and the methods used to develop the code seems to be sound. Initially the transient 3-D incompressible laminar lid-driven flow in a cubic cavity is computed through the developed code for code validation and to show the performance of multigrid.

Table 1 Performance of multigrid on a 65 × 65 ×65 grid at $Re=1000$ for a single sided lid-driven cubic cavity

Time-steps ($\Delta t=0.001$)	CPU time (min)		Speed-up
	Single-grid	MG 4-level	
100	311	26	11.96
500	1 407	80	17.55

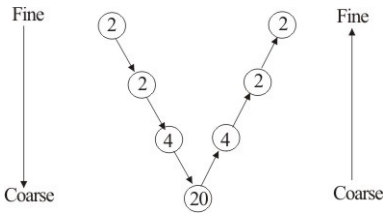


Fig.1(a) V-cycle multigrid showing iterations at various levels

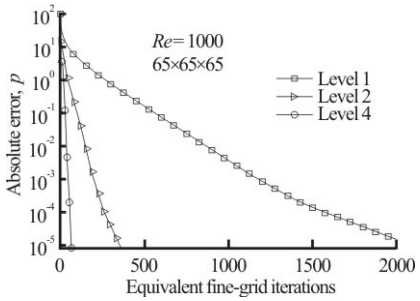


Fig.1(b) Pressure error history at $t=0.1$ for the Poisson equation at $Re=1000$

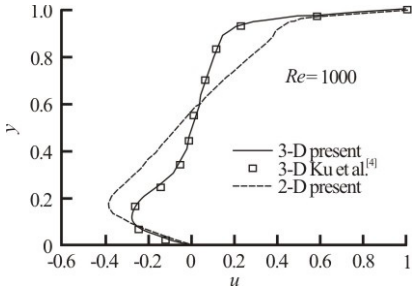
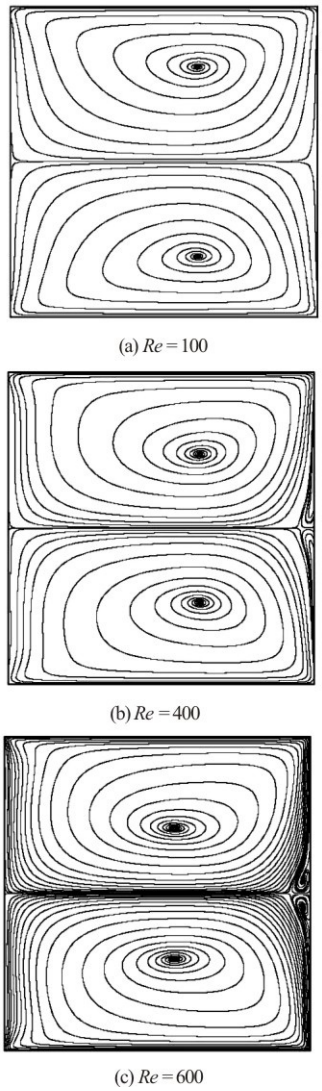


Fig.2 Comparison of steady-state horizontal velocity along the vertical centerline for $Re=1000$ at $z=0.5$ for the single-sided cubic cavity

In the present study a 4-level V-cycle multigrid shown in Fig.1(a) has been used in all the computations to solve the pressure Poisson equation and the number of sweeps used in various grid-levels is given inside the corresponding circles. At $Re=1000$ on a 65 × 65 × 65 grid, it is observed that using four levels is good enough and a further increase of level produces no time-wise gain. To gain an insight into the convergence behavior after 100 time steps, at $t=0.1$ a plot between the pressure error and number of iterations required to solve the pressure Poisson equation is shown in Fig.1(b). Before examining overall quantitative performance data, it is instructive to consider the convergence histories in Fig.1(b) obtained with the single grid and with the sequences of 2- and 4-levels. Expectedly the convergence curves relating to multigrid are considerably steeper than those relating to the single grid. The ratio of the computational effort in work units for the single grid to that for the multigrid may be termed speed-up. As the convergence limit of error is lowered speed-up is seen to increase. This is because on a single grid, error-reduction rate becomes smaller and smaller as the iteration progresses whereas multigrid maintains more or less the same error-reduction rate throughout. The speed-up achieved by the 4-level multigrid is represented in

Table 1. The CPU times of multigrid and single-grid computations to reach $t = 0.1$ and $t = 0.5$ for $Re = 1000$ are shown in Table 1. For the same fall of residual, time gain by multigrid is impressive. Figure 2 shows the steady-state velocity profile of the u-component on the vertical centreline at the plane $z = 0.5$ at $Re = 1000$. The results show an excellent match with those of Ku etal.[4]. The 2-D results are also shown for comparison.



(a) $Re = 100$

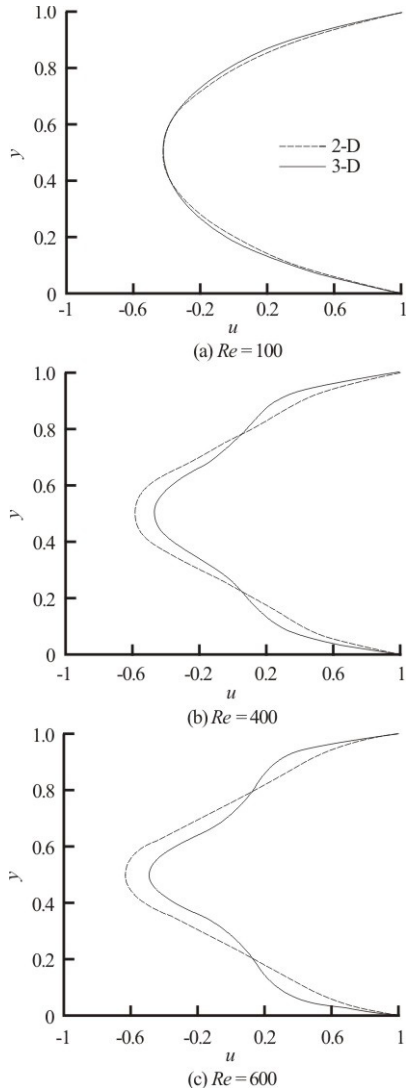
(b) $Re = 400$

(c) $Re = 600$

Fig.3 Steady-state projected streamline patterns for different Re's for the facing-wall two-sided cubic lid-driven cavity flow on a 65 × 65 × 65 grid

The results presented in the preceding section show the accuracy and the capability of the present code to accurately compute transient viscous flows. After having thus gained confidence in the code, it is then applied to compute a hitherto unexplored flow configuration. The problem consists of a cubic cavity filled with a stationary fluid that is set into motion by the sudden simultaneous movement of the top and the bottom walls from the left to right. The physical boundary conditions of the geometry are specified for $t \geq 0$ as

(1) At $x = 0$ and 1, $u = v = w = 0$.
(2) At $z = 0$ and 1, $u = v = w = 0$.
(3) At $y = 0$, $u = 1$, $v = 0$, $w = 0$.
(4) At $y = 1$, $u = 1$, $v = 0$, $w = 0$.



(a) $Re = 100$

(b) $Re = 400$

(c) $Re = 600$

Fig.4 Steady-state horizontal velocity along the vertical centreline for the facing-wall two-sided cubic lid-driven cavity flow for Re = 100, 400 and 600 at $z = 0.5$

The reason for selecting this flow configuration for numerical study is that this geometry involves interesting flow features including gradual development of a free-shear layer and associated off-corner secondary vortices. The use of a grid with appropriate clustering and the use of multigrid suggest that the present computations combine accuracy, space-grid economy and time-wise efficiency. As has already been mentioned the flow in a cubic cavity with two-sided parallel wall movement has not been

examined so far.

We compute the flow in this geometry using a grid of similar size (65 × 65 × 65) but clustering points not only in the wall shear layers but also in the free-shear layer mid-way between the moving walls. Computations are carried out for $Re = 100$, 400 and 600. Figures 3(a) - 3(c) show the steady-state streamline patterns asymptotically obtained from the present transient computations in the $z = 0.5$ plane (x being the direction of wall movement as in the case of single-sided cavity). Figure 3(a) shows that at $Re = 100$ two counter-rotating primary vortices appear and there is no trace of any near-wall secondary vortices. At $Re = 400$ (Fig.3(b)), apart from the primary vortices a counter-rotating pair of small secondary vortices symmetrically placed about the horizontal cavity centerline is seen to appear near the centre of the right wall. Also a free shear-layer about this centerline is now more prominent. Figure 3(c) shows the streamline pattern for $Re = 600$. It is seen that the size of the secondary vortices increases significantly with an increase in the Reynolds number. It is also seen that with an increase in Re the distance of the top and bottom primary vortex cores from the top- and bottom-right corners increases and at $Re = 600$ they take position near the centers of the top and bottom halves of the cavity. The counter-rotating pairs of primary and secondary vortices maintain their symmetry about the horizontal centerline for all the Reynolds numbers. Beya and Lili[8] pointed out that for a 3-D two-sided non-facing lid-driven cavity at $Re = 600$ the flow is not steady and periodic solution exists, whereas for the two-sided lid-driven cubic cavity with parallel wall motion we find that there exists a unique, steady and stable solution. In order to distinguish between the 2-D and 3-D steady-flow patterns, 3-D midspan ($z = 0.5$) velocity profiles are compared with a 2-D situation in Fig.4. Figure 4 shows the variation of velocity component u along the vertical centerline ($x = 0.5$). At $Re = 100$ the deviation between 2-D and 3-D results (Fig.4(a)), though small, is good enough to indicate that sidewall effects can be perceived at mid-span even at relatively low Reynolds numbers. Similar to the single-sided cavity studied earlier, as Re increases to 400 and 600 the deviations between 2-D and 3-D results at the mid-span increases (Fig.4(b)-4(c)). Again like the single-sided lid-driven cubic cavity the magnitude of the velocity components for the 3-D flow are lower than those of the 2-D flow owing to the 3-D effect of the side walls. This reduction in magnitude increases with an increase in Re.

The transient problem of the two-sided cubic cavity flow studied here consists in the impulsive movement of the top and bottom walls from the left to right. The initial velocity field is obtained by taking u, v and w as zero at all grid-nodes except those on the top and the bottom moving walls where u is taken as unity, v and w as zero. Thus at $t = 0$ we start from a divergence-free flow, which is a necessary condition to be satisfied by an incompressible flow at every instant. To ensure time-accuracy time steps chosen are so small as to make the results time-step independent. Figure 5 depicts, at midspan ($z = 0.5$), the time-wise evolution of the streamline patterns at $Re = 600$ till the steady state is reached. Figure 5(a) shows the streamline pattern at $t = 1.0$ when the primary vortex cores are seen close to the top right and bottom right corner symmetric to each other about the horizontal centerline. At this instant the secondary vortices have not developed as yet. At time $t = 3.0$ (not shown in figure) the two primary vortex cores are seen to move away from the nearest corners maintaining their symmetry about the horizontal centerline. Also seen at this instant is the emergence of a pair of two counter-rotating secondary vortices symmetrically placed about the horizontal centerline near the center of the right wall. At time $t = 5.0$ (Fig.5(b)) the primary vortex cores are seen to continue to move away from their nearest corners whereas the size of the pair of secondary vortices enlarges. The movement of the primary vortex cores away from the respective corners of origin is seen to continue and reach near the centers of the top and bottom halves but the secondary vortex sizes do not change much compared with those at $t = 5.0$. For a fall of mass residual below 10^{-5} the steady state is reached at time $t = 42.8$. At this steady state (Fig.5(c)), the two counter-rotating primary vortex cores are stably positioned. The top one is located slightly below the geometric centre of the upper half and the bottom one slightly above the geometric center of the lower half of the cavity. Also there are no appreciable changes in the positions and shapes of the counter-rotating pair of secondary vortices. Observing these figures in the chronological sequence also reveals that the flow gradient in the free shear-layer about the horizontal centerline of the cavity becomes sharper with time. Because of grid clustering at wall and free shear-layer, the second-order temperal accuracy and higher-order spatial accuracy of the scheme and the care taken to maintain time-step-independence of the results throughout, the obtained transient computations for this hitherto unexamined flow configuration are highly reliable. Use of high precision arithmetic to avoid possible accumulation of the round-off errors lends further credibility to the results. The time-wise efficiency of the transient computations is also high as multigrid has been used to a good effect. Overall these results are produced accurately and efficiently with grid economy.

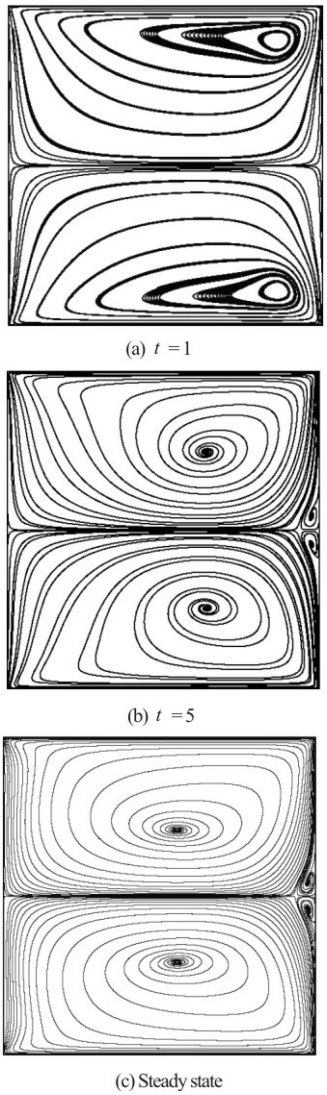


Fig.5 Time evolution of projected streamlines for the facing-wall two-sided cubic lid-driven cavity flow at $Re = 600$

7. Conclusion

The present work deals with the development and application of a multigrid-accelerated 3-D code that accurately and efficiently computes incompressible transient viscous flows especially in geometries that allow the graded Cartesian meshes to be used conveniently to resolve the sharp gradients in shear layers by locally clustering the grid there. A fractional-step method is used to obtain second-order temporal accuracy and spatial discretizations of the convective and viscous terms are of third-and fourth-order spatial accuracy, respectively. The time-consuming process of computation of the Poisson equation at every time step is accelerated by using a V-cycle multigrid approach. For accurate implementation of the multigrid method, the finite difference discretization and grid transformation of the graded Cartesian meshes are employed. First, computations of transient and steady-state flows are carried out for the single-sided lid-driven cubical cavity. After having used the code to compute the flow in the single-sided cubical cavity to establish its credibility, it is then used to compute transient and steady-state flows in a hitherto unexplored configuration, namely, the two-sided cubical cavity flow induced by the motion of two facing walls in the same direction. The grid here is clustered not only near the walls but also in the free-shear layer midway between the moving walls to obtain a good grid-economy. It is observed that for the nonfacing two-sided cubic cavity, flow becomes periodic at $Re = 540$. For the facing wall two-sided cubic cavity, however, steady solutions are obtained much beyond this Reynolds number and steady and transient results are presented here also for such values of *Re*. Various observations are made about this untested flow configuration. As all the steady-state results are grid independent, the transient results are time-step independent produced on the same grids and the accuracy of the spatio-temporal discretization is sufficiently high, all the steady and transient results reported for this new flow configuration are likely to be highly reliable and accurate. As has already been mentioned the results are also produced with good grid economy and time-wise efficiency. These results can thus serve as a means of verifying the performance of various algorithms that can be applied to the new test problem we propose. The code developed for the present transient computations can also be effectively used for various other 3-D rectangular geometries. It will, therefore, not be out of place to mention here that the code may have the potential of being gainfully used for LES and DNS in those geometries that allow effective use of the graded Cartesian meshes.

References

[1] KOSEFF J. R., STREET R. L. The lid-driven cavity flow: A synthesis of qualitative and quantitative observations[J]. **Journal of Fluids Engineering,** 1984, 106(4): 390-398.

[2] AUTERI F., PAROLINI N. and QUARTAPELLE L. Numerical investigation on the stability of singular driven cavity flow[J]. **Journal of Computational Physics,** 2002, 183(1): 1-25.

[3] KOSEFF J. R., STREET R. L. On endwall effects in a lid-driven cavity flow[J]. **Journal of Fluids Engineering,** 1984, 106(4): 385-389.

[4] KU H. C., HIRSH R. S. and TAYLOR T. D. A pseudospectral method for solution of the three-dimensional incompressible Navier-Stokes equations[J]. **Journal of Computational Physics,** 1987, 70(2): 439-462.

[5] DING H., SHU C. and YEO K. S. et al. Numerical computation of three-dimensional incompressible viscous flows in the primitive variable form by local multiquadric differential quadrature method[J]. **Computer Methods in Applied Mechanics and Engineering,** 2006, 195(7-8): 516-533.

[6] TANG L. Q., CHENG T. and TSANG T. T. H. Transient solutions for three-dimensional lid-driven cavity flows by a least-squares finite element method[J]. **International Journal of Numerical Methods and Fluids,** 1995, 21(5): 413-432.

[7] GUERMOND J. L., MIGEON C. and PINEAU G. et al. Start-up flows in a three-dimensional rectangular driven cavity for aspect ratio 1:1:2 at *Re* = 1000[J]. **Journal of Fluid Mechanics,** 2002, 450: 169-199.

[8] BEYA B. B., LILI T. Three-dimensional incompressible flow in a two-sided non-facing lid-driven cubical cavity[J]. **Comptes Rendus Mecanique,** 2008, 336(11-12): 863-872.

[9] CHORIN A. J. A numerical method for solving incompressible viscous flow problem[J]. **Journal of Computational Physics,** 1967, 2(1): 12-26,.

[10] KIM J., MOIN P. Application of a fractional-step method to incompressible Navier-Stokes equation[J]. **Journal of Computational Physics,** 1985, 59(2): 308-323.

[11] AI Cong-fang and JIN Sheng. Three-dimensional non-hydrostatic model for free-surface flows with unstructured grid[J]. **Journal of Hydrodynamics,** 2008, 20(1): 108-116.

[12] GAO Wei, DUAN Ya-li and LIU Ru-xun. The finite volume projection method with hybrid unstructured triangular collocated grids for incompressible flows[J]. **Journal of Hydrodynamics,** 2009, 21(2): 201-211.

[13] TANNNEHILL J. C., ANDERSON D. A. and PLETCHER R. H. **Computational fluid mechanics and heat transfer**[M]. Second Edition, New York: Hemisphere Publishing Corporation, 1984.

[14] KAWAMURA T., TAKAMI H. and KUWAHARA K. Computation of high Reynolds number flow around a circular cylinder with surface roughness[J]. **Fluid Dynamics Research,** 1986 , 1(2): 145-162.

[15] KUMAR D. S., DASS A. K. and DEWAN A. A multigrid-accelerated code on graded Cartesian meshes for 2D time-dependent incompressible viscous flows[J]. **Engineering Applications of Computational Fluid Mechanics,** 2010, 4(1): 71-90.